Science Signaling
AAAS

www.sciencesignaling.org/cgi/content/full/12/562/eaat6662/DC1

# Supplementary Materials for

## Activation of atypical protein kinase C by sphingosine 1-phosphate revealed by an aPKC-specific activity reporter

Taketoshi Kajimoto*, Alisha D. Caliman, Irene S. Tobias, Taro Okada, Caila A. Pilo, An-Angela N. Van, J. Andrew McCammon, Shun-ichi Nakamura, Alexandra C. Newton*

*Corresponding author. Email: anewton@ucsd.edu (A.C.N.); tkajimot@med.kobe-u.ac.jp (T.K.)

Published 1 January 2019, *Sci. Signal.* **12**, eaat6662 (2019)
DOI: 10.1126/scisignal.aat6662

**This PDF file includes:**

Fig. S1. Phosphatase sensitivity of aCKAR is greater than that of CKAR.
Fig. S2. S1P signaling does not affect the Par6-regulated basal activity of PKCζ in breast cancer cells.
Fig. S3. Identification of critical sites and amino acids for PKCι-S1P binding in silico.
Fig. S4. Apoptotic nuclear morphology images.

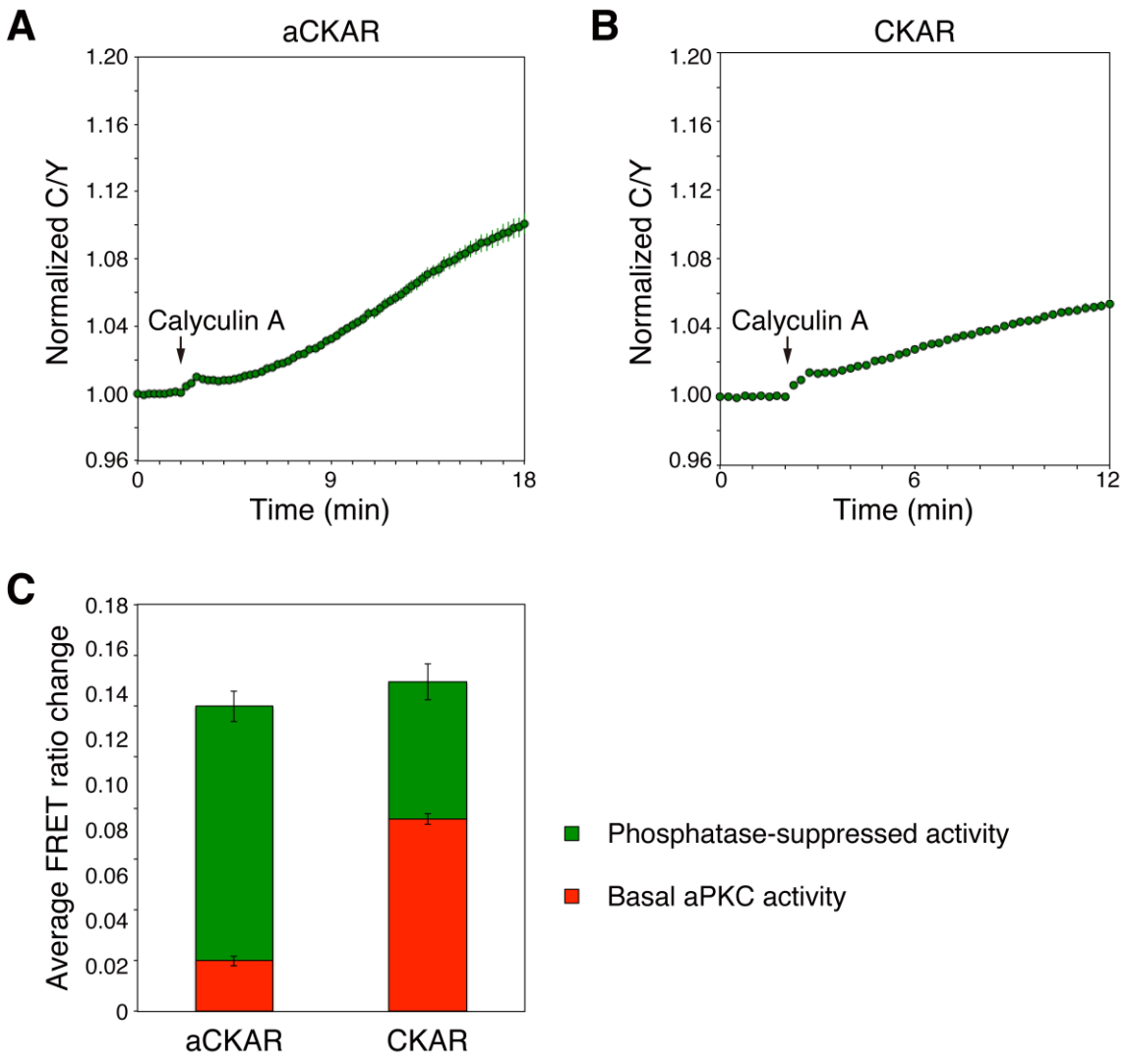


**Fig. S1. Phosphatase sensitivity of aCKAR is greater than that of CKAR.** (**A**) COS7 cells were co-transfected with aCKAR and mCherry-PKMζ. The CFP/YFP FRET (C/Y) emission ratio was quantified as a function of time following the addition of Calyculin A (50 nM). Data represent the C/Y emission ratio normalized to the starting point (1.0) with means ± S.E. (n = 55 cells). (**B**) As in (A), except the cells were transfected with CKAR. Data represent the C/Y emission ratio normalized to the starting point (1.0) with means ± S.E. (n = 56 cells). (**C**) Approximation of phosphatase-suppressed (green) and inhibitor-sensitive (red) aPKC activities measured using aCKAR or CKAR in COS7 cells overexpressing the constitutively active mCherry-PKMζ. The phosphatase-suppressed activity represents the average FRET ratio change calculated by averaging the last 1 min of normalized C/Y emission ratio in (A) and (B); the basal aPKC activity is from Fig. 1B. This dynamic range of 0.14 is similar to our previously reported value for PKCλ measured using CKAR (*10*).

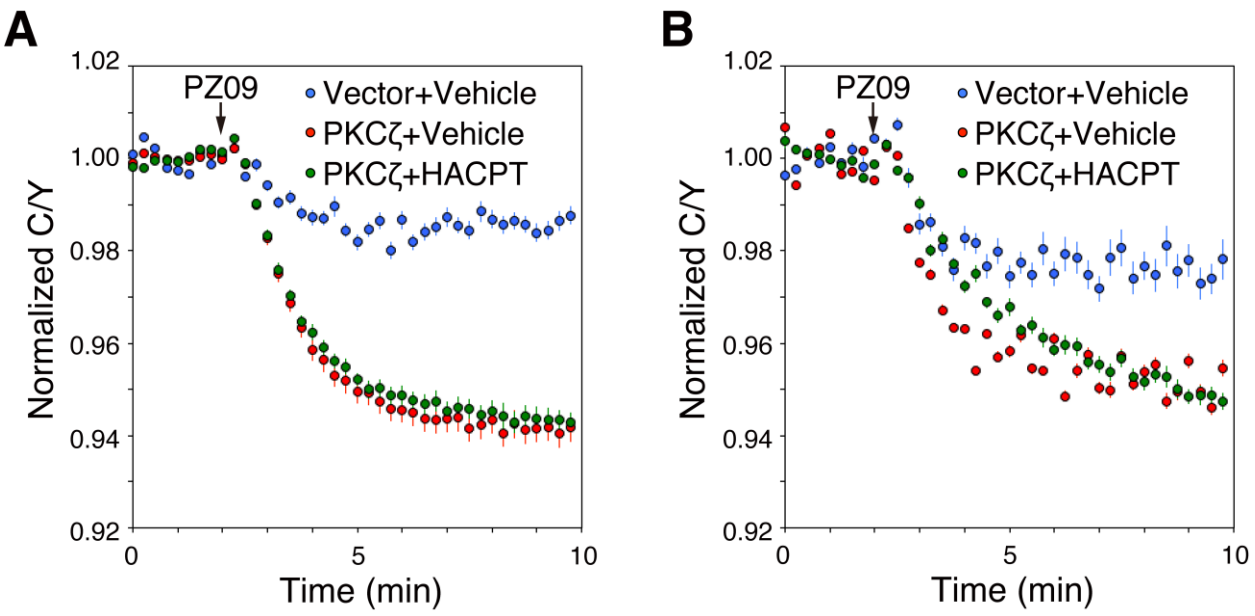


**Fig. S2. S1P signaling does not affect the Par6-regulated basal activity of PKCζ in breast cancer cells. (A and B)** MDA-MB-231 cells (A) or MCF7 cells (B) were co-transfected with the CKAR fused to the PB1 domain of Par6 (CKAR-PB1$^{Par6}$) and mCherry (Vector) or mCherry-PKCζ (PKCζ). Cells were pre-treated with DMSO vehicle or 5 μM HACPT for 16 h and then treated with 5 μM PZ09 during live-cell imaging. The normalized C/Y emission ratio was quantified as a function of time following PZ09 treatment. Data represent the means ± S.E., n ≥ 23 cells for (A**)**, n ≥ 20 cells for (B**)**.

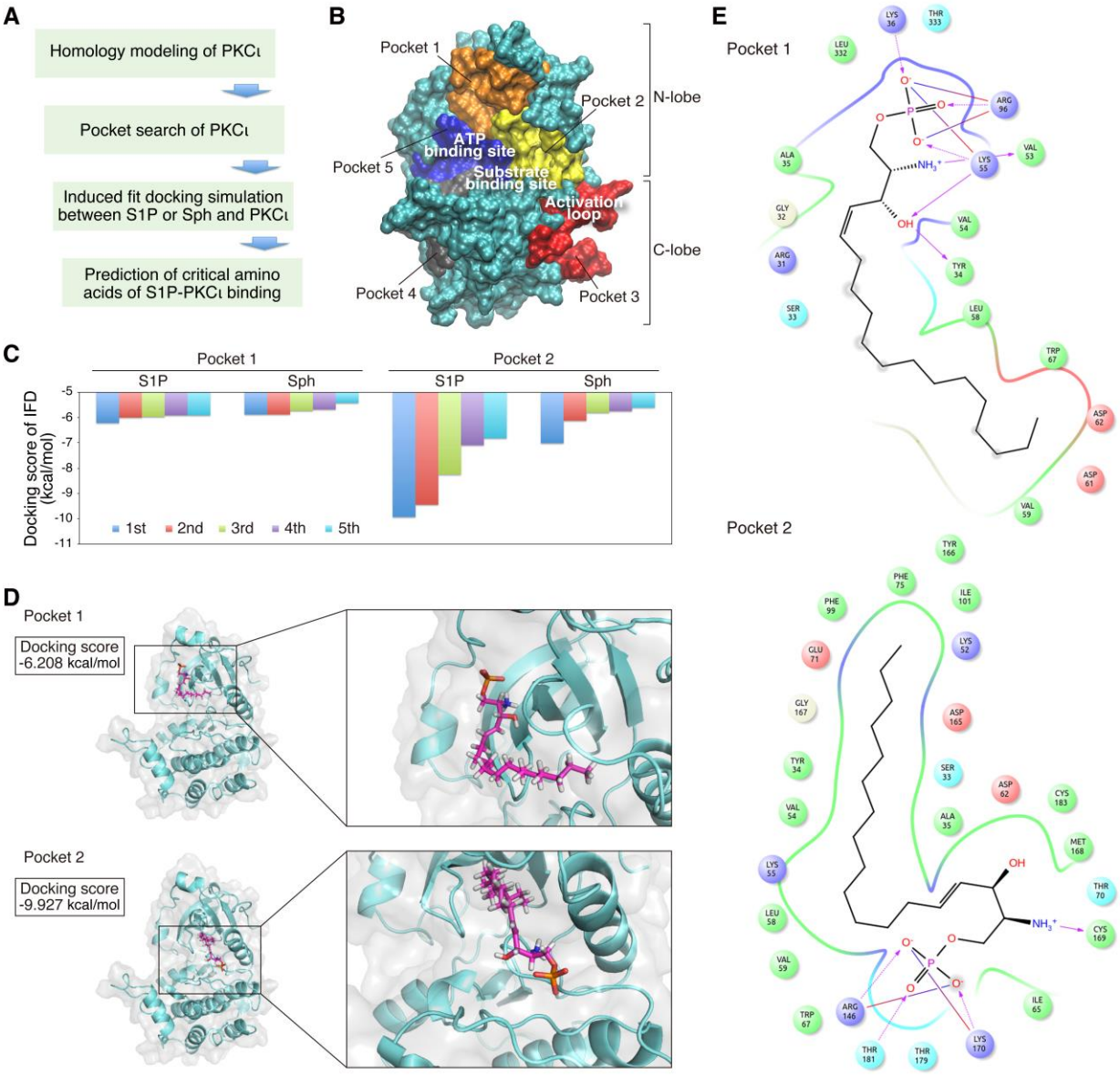


**Fig. S3. Identification of critical sites and amino acids for PKCι-S1P binding in silico.** (**A**) Flowchart of the strategy for identifying the critical sites and amino acids of PKCι for S1P binding. (i) Homology modeling of catalytic domain of PKCι from crystal structure of PKCι; (ii) a search of potential ligand-binding pockets of PKCι; (iii) induced fit docking simulation between S1P or Sph and catalytic domain of PKCι; and (iv) identification of candidate critical pockets and amino acids for S1P-PKCι binding. (**B**) The search for ligand binding pockets on the surface of the homology model for the catalytic domain of PKCι, as depicted, was performed using the Schrödinger package. (**C**) S1P or sphingosine (Sph) was docked to the center of mass position of pocket 1 or pocket 2 on the catalytic domain of PKCι using an induced fit docking protocol in the Schrödinger package. The five lowest docking scores (kcal/mol) from the induced fit docking protocol were shown for each site. IFD: induced fit docking. (**D**) Induced fit

docking pose of S1P (carbon atoms in pink) to pocket 1 or pocket 2, and the catalytic domain of human PKCι are shown with docking score. These docking poses are from the first place of docking score for each pocket. (**E**) Two-dimensional interaction diagram of the S1P-PKCι binding as in (D**)** are shown. Negatively charged, positively charged, polar, hydrophobic, and glycine residues at the active site are represented by red, purple, cyan, green, and white spheres, respectively. Hydrogen bonds between the S1P and backbone or side chains are shown in solid pink arrows or dashed pink arrows, respectively. Salt bridges are shown in red-blue lines. $Lys^{36}$, $Lys^{55}$, and $Arg^{96}$ in the pocket 1 correspond to $Lys^{267}$, $Lys^{286}$, and $Arg^{327}$ of full length PKCι. $Arg^{146}$ and $Lys^{170}$ in the pocket 2 correspond to $Arg^{377}$ and $Lys^{401}$ of full length PKCι.

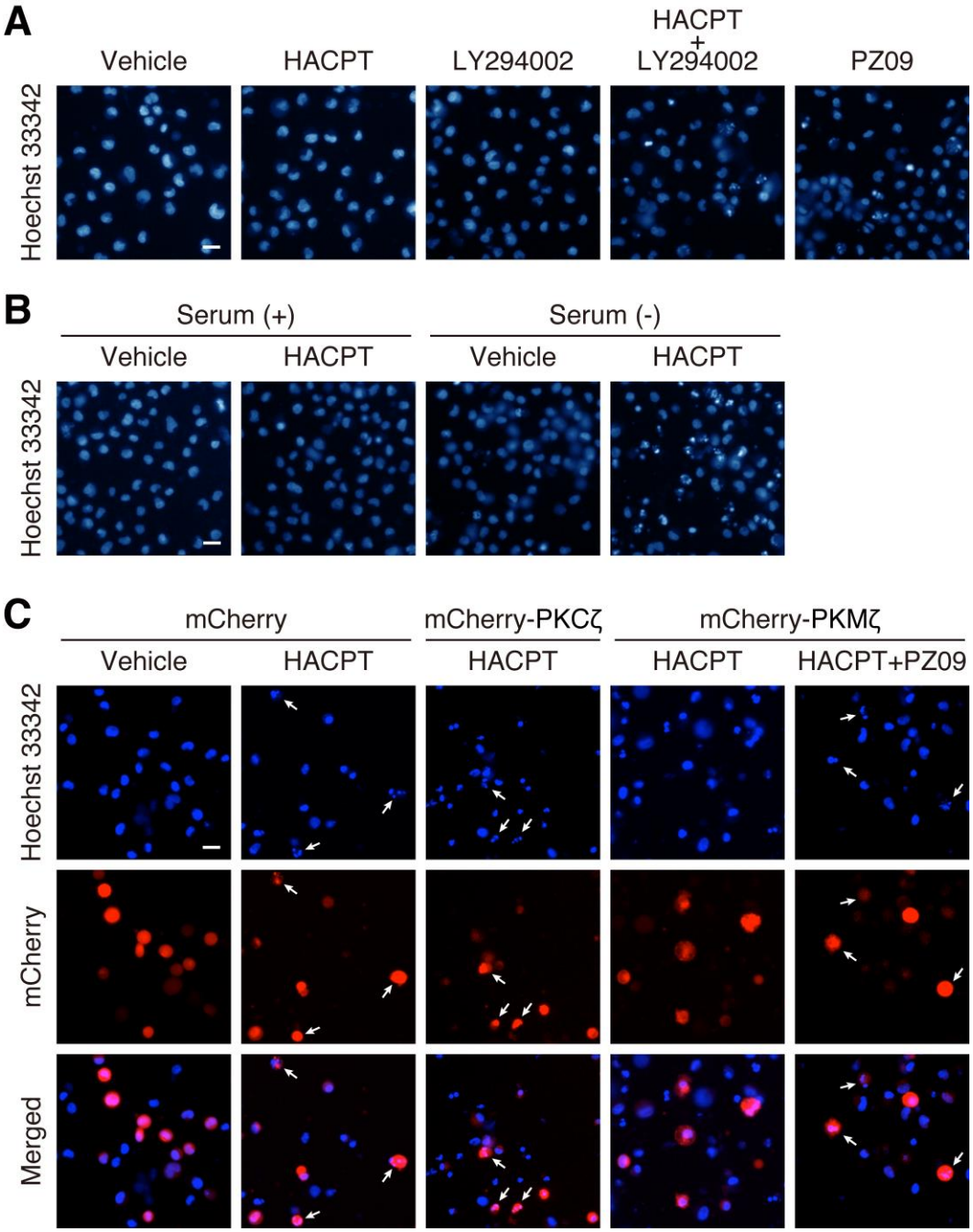


**Fig. S4. Apoptotic nuclear morphology images.** (**A**) Hoechst 33342 fluorescent images for chromatin condensation and nuclear fragmentation corresponding to Fig. 7C. Scale bar, 20 μm. (**B**) Hoechst 33342 fluorescent images for chromatin condensation and nuclear fragmentation corresponding to Fig. 7F. Scale bar, 20 μm. (**C**) Hoechst 33342 fluorescent images for chromatin condensation and nuclear fragmentation corresponding to Fig. 7I. Arrows indicate apoptotic cells within the population of mCherry-positive cells. Scale bar, 20 μm.